Jets, bulk matter, and their interaction in heavy ion collisions at several TeV

K. Werner,[1] Iu. Karpenko,[2] M. Bleicher,[3] T. Pierog,[4] and S. Porteboeuf-Houssais[5]

[1]*Laboratoire de Physique Subatomique et des Technologies, University of Nantes, CNRS-IN2P3, Ecole des Mines de Nantes, Nantes, France*
[2]*Bogolyubov Institute for Theoretical Physics, Kiev 143, 03680, Ukraine*
[3]*Frankfurt Institute for Advanced Studies, Johann Wolfgang Goethe Universitaet, Frankfurt am Main, Germany*
[4]*Karlsruhe Institute of Technology, Campus North, Institut für Kernphysik, Germany*
[5]*Laboratoire de Physique Corpusculaire, Université Blaise Pascal, CNRS-IN2P3, Clermont-Ferrand, France*

We discuss a theoretical scheme that accounts for bulk matter, jets, and the interaction between the two. The aim is a complete description of particle production at all transverse momentum (p_t) scales. In this picture, the hard initial scatterings result in mainly longitudinal flux tubes, with transversely moving pieces carrying the p_t of the partons from hard scatterings. These flux tubes constitute eventually both bulk matter (which thermalizes and flows) and jets. We introduce a criterion based on parton energy loss to decide whether a given string segment contributes to the bulk or leaves the matter to end up as a jet of hadrons. Essentially low p_t segments from inside the volume will constitute the bulk, high p_t segments (or segments very close to the surface) contribute to the jets. The latter ones appear after the usual flux tube breaking via q-qbar production (Schwinger mechanism). Interesting is the transition region: Intermediate p_t segments produced inside the matter close to the surface but having enough energy to escape, are supposed to pick up q-qbar pairs from the thermal matter rather than creating them via the Schwinger mechanism. This represents a communication between jets and the flowing bulk matter (fluid-jet interaction). Also very important is the interaction between jet hadrons and the soft hadrons from the fluid freeze-out. We employ this picture to investigate Pb-Pb collisions at 2.76 TeV. We discuss the centrality and p_t dependence of particle production and long-range dihadron correlations at small and large p_t.

　　　　　　　　　　　　　　　　PACS number(s): 25.75.−q

I. INTRODUCTION

Traditionally the physics of ultrarelativistc heavy ion collisions is discussed in terms of different categories such as collective dynamics, parton-jet physics, and fluctuation-correlation studies, although these different topics are highly correlated. In this article, a complete dynamical picture of particle production at all p_t scales will be presented, which accounts for the production and evolution of bulk matter and jets, and the very important interaction between the two components (which is not only the well known parton energy loss). The consequences of these interactions can be nicely seen in long-range dihadron correlations.

The physical picture of our approach is the following: Initial hard scatterings result in mainly longitudinal flux tubes, with transversely moving pieces carrying the p_t of the partons from hard scatterings. These flux tubes constitute eventually both bulk matter (which thermalizes, flows, and finally hadronizes) and jets, according to some criteria based on partonic energy loss. We will consider a sharp fluid freeze-out hypersurface, defined by a constant temperature. Freeze-out here simply means the end of the fluid phase, but the hadrons still interact. High-energy flux-tube segments will leave the fluid, providing jet hadrons via the usual Schwinger mechanism of flux-tube breaking caused by quark-antiquark production.

But the jets may also be produced at the freeze-out surface. Here we assume that the quark-antiquark needed for the flux tube breaking is provided by the fluid, with properties (momentum, flavor) determined by the fluid rather than the Schwinger mechanism. Considering transverse fluid velocities up to 0.7c, and thermal parton momentum distributions, one

may get a push of a couple of GeV to be added to the transverse momentum of the string segment. This will be a crucial effect for intermediate p_t jet hadrons.

There is another important issue. Even for hadrons with transverse momenta of 10–20 GeV, there is a large probability of a jet hadron formation before it enters the dense hadronic medium. This means a significant probability of scatterings between jet hadrons and soft hadrons (from freeze-out), having essentially two consequences: an increase of low p_t particle production, and a reduction of yields at high p_t. In addition there are of course the well known hadronic interactions between the soft hadrons.

We have discussed different processes that all affect p_t spectra. It is, however, possible to disentangle different contributions, by looking at dihadron correlations. These are extremely useful tools heavily used by experimental groups at the RHIC and the LHC [1–5]. Recently, the CMS and ALICE collaborations published results on such correlations in Pb-Pb collisions at 2.76 GeV and different centralities, over a more or less broad range in relative pseudorapidity ($\Delta\eta$) and full coverage of the relative azimuthal angle ($\Delta\phi$) [4,5]. Different combinations of transverse momenta p_t^{assoc} and p_t^{trigg} of associated and trigger particles in the range between 0.25 GeV/c and 15 GeV/c are investigated. Considering long-range correlations ($|\Delta\eta| > A$, $A \geqslant 0.8$), the coefficients $V_{n\Delta}$ of the harmonic decomposition factorize as $V_{n\Delta} = v(p_t^{\mathrm{assoc}}) v(p_t^{\mathrm{trigg}})$, not only for small transverse momenta but also for example for large p_t^{trigg} and small p_t^{assoc}. For small momenta the situation seems to be clear: the correlation is flow dominated. But factorization does not necessarily mean that both hadrons carry the flow from the fluid. This can in

particular not be the answer for observed correlations for large p_t^{trigg}; here we have to deal with an interaction between the flowing bulk and jets, which makes the observed correlations very interesting in particular as a test of our ideas concerning bulk-jet separation and interaction.

Another challenge: The ATLAS collaboration showed recently results [6] on elliptical flow of charged particles with respect to an event plane in the opposite η hemisphere (also a kind of long-range correlation). The v_2 values are quite large up to values of $p_t = 20$ GeV/c, for eight different centrality ranges. Can we understand this in a quantitative fashion?

The heavy ion results shown in this paper are based on 2 000 000 events simulated with EPOS2.17V3. A central (0–5%) Pb-Pb event takes on the average around 2 HS06 hours CPU time, using machines with an average scaling factor of 8.7 [7]. Always six events share the same parton configuration and hydrodynamic evolution, with only particle production and hadronic rescattering being redone (to gain statistics). This is taken care of when considering mixed events in correlation studies.

II. BASIS: FLUX TUBES FROM A MULTIPLE SCATTERING APPROACH

The starting point is a multiple scattering approach corresponding to a marriage of Gribov-Regge theory and perturbative QCD (pQCD) (see Fig. 1). An elementary scattering corresponds to a parton ladder, containing a hard scattering calculable based on pQCD, including initial and final state radiation (for details see Ref. [8]). These ladders are identified with flux tubes, see Fig. 2 which are mainly longitudinal objects, with transversely moving parts, carrying the transverse momenta of the hard scatterings. These objects are also referred to as kinky strings. One should note that here multiple scattering does not mean just a rescattering of hard partons, it rather means a multiple exchange of complete parton ladders, leading to many flux tubes. In this case, the energy sharing between the different scatterings will be very important, to be discussed later.

The consistent quantum mechanical treatment of the multiple scattering is quite involved; it is based on cutting rule
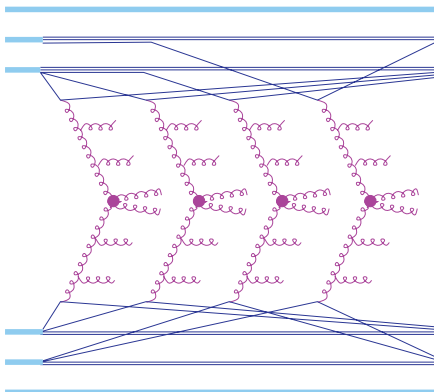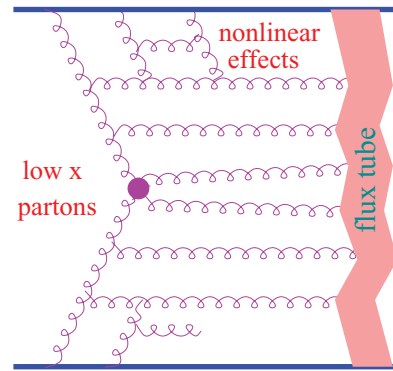

FIG. 2. (Color online) An elementary parton ladder, whose final state is identified with a color flux tube (kinky string).

techniques to obtain partial cross sections, which are then simulated with the help of Markov chain techniques [9].

As said before, the final state partonic system corresponding to elementary parton ladders are identified with flux tubes. The relativistic string picture [10–12] is very attractive, because its dynamics is essentially derived from general principles as covariance and gauge invariance. The simplest possible string is a surface $X(\alpha, \beta)$ in $3+1$ dimensional space-time, with piecewise constant initial velocities $\partial X/\partial \beta$. These velocities are identified with parton velocities, which provide a one to one mapping from partons to strings. For details see Refs. [8,9]. The high transverse momentum (p_t) partons will show up as transversely moving string pieces [see Fig. 3(a)]. Despite the fact that in the TeV energy range most processes are hard, and despite the theoretical importance of very high p_t partons, it should not be forgotten that the latter processes are rare, most kinks carry only few GeV of transverse momentum, and the energy is nevertheless essentially longitudinal. In case of elementary reactions, the strings will break [see Fig. 3(b)] via the production of quark-antiquark pairs according to the
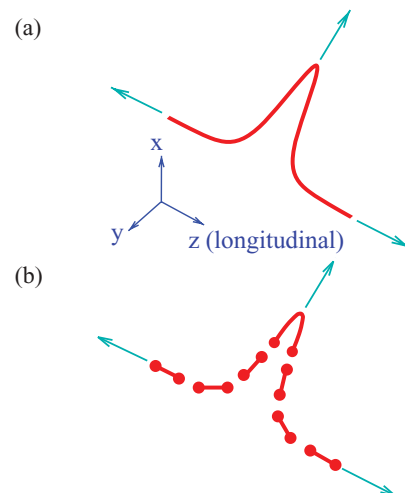

FIG. 3. (Color online) (a) Flux tube with transversely moving part (kinky string) in space, at given proper time. (b) Flux-tube breaking via q-$\bar{q}$ production, which screens the color field (Schwinger mechanism).

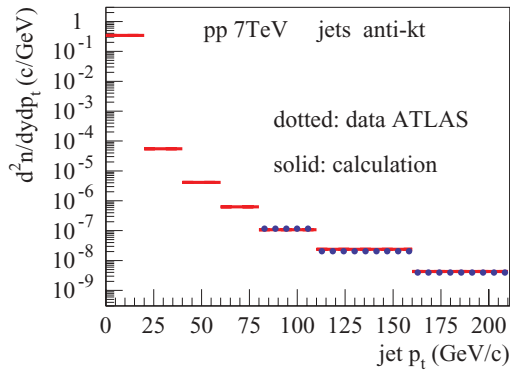FIG. 1. (Color online) Multiple scattering in nucleus-nucleus collisions.

FIG. 4. (Color online) Inclusive p_t distribution of jets. We show the calculation (full lines) compared to ATLAS data [18] (dotted lines).

so-called area law [8,9,13,14]. The string segments are identified with final hadrons and resonances.

This picture has been very successful to describe particle production in electron-positron annihilation or in proton-proton scattering at very high energies. In the latter case, not only low p_t particles are described correctly, for example for pp scattering at 7 TeV [15,16], also jet production is covered. As discussed earlier, the high transverse momenta of the hard partons show up as kinks, transversely moving string regions. After string breaking, the string pieces from these transversely moving areas represent the jets of particles associated with the hard partons. To demonstrate that this picture also works quantitatively, we compute the inclusive p_t distribution of jets, reconstructed with the anti-kt algorithm [17] and compare with data [18] (see Fig. 4). In Fig. 5, we compare our p_t distribution of partons with a parton model calculation based on CTEQ6 parton distribution functions [19], in both cases leading order with a K factor of 2.

III. JET-BULK SEPARATION

In heavy ion collisions and also in high multiplicity events in proton-proton scattering at very high energies, the density of strings will be so high that the strings cannot decay
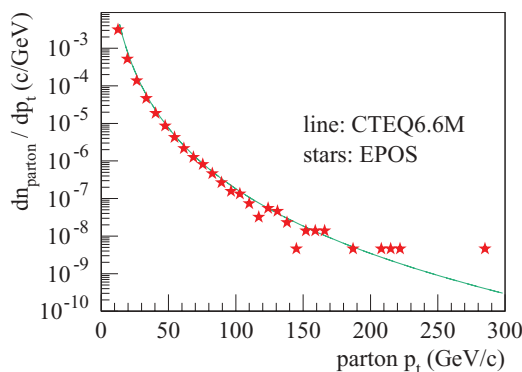

FIG. 5. (Color online) Transverse momentum distribution of partons: We compare our results (red stars) with a parton model calculation (dotted line).
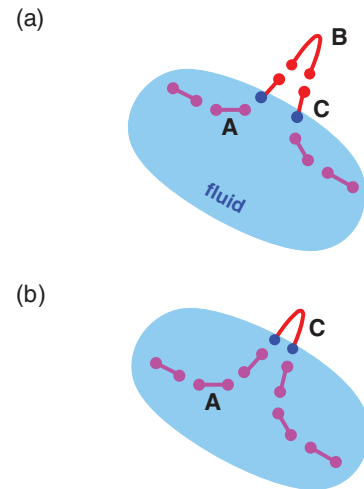

FIG. 6. (Color online) Flux tube in matter (from other flux tubes, blue colored area). One distinguishes three types of behavior for string segments, noted as A, B, C (see text). The highest p_t string segment may be (a) of type B or (b) of type C.

independently as described above. Here we have to modify the procedure as discussed in the following. The starting point are still the flux tubes (kinky strings) originating from elementary collisions. These flux tubes will constitute both bulk matter, which thermalizes and expands collectively, and jets. The criterion that decides whether a string piece ends up as bulk or jet will be based on energy loss. In the following we consider a flux tube in matter, where matter first means the presence of a high density of other flux tubes, which then thermalize. A more quantitative discussion will follow.

Three possibilities should occur, referred to as A, B, C (see Fig. 6):

  (i) String segments far from the surface and/or being slow will simply constitute matter, they lose their character as individual strings. This matter will evolve hydrodynamically and finally hadronize (soft hadrons).
 (ii) Some string pieces (like those close to transversely moving kinks) will be formed outside the matter, they will escape and constitute jets (jet hadrons).
(iii) There are finally also string pieces produced inside matter or at the surface, but having enough energy to escape and show up as jets (jet hadrons). They are affected by the flowing matter (fluid-jet interaction).

Let us discuss how the above ideas are realized. In principle the formation and expansion of matter and the interaction of partons with matter is a dynamical process. However, the initial distribution of energy density and the knowledge of the initial momenta of partons (or string segments) allows already an estimate about the fate of the string segments. By initial time we mean some early proper time τ_0 which is a parameter of the model. Strictly speaking, energy loss concerns partons, modifying eventually the kink momenta in our picture, and the momenta of the string segments after breaking will be reduced. We will therefore base our discussion on energy loss on string segments.

We estimate the energy loss ΔE of string segments along their trajectory to be

$$\Delta E = k_{\text{Eloss}} \, E_0 \int (\rho V_0)^{3/8} \max(1, \sqrt{E/E_0}) \, dL/L_0, \quad (1)$$

inspired by Ref. [20], where ρ is the density of string segments at initial proper time τ_0, V_0 is an elementary volume cell size (technical parameter, taken to be $0.147 \, \text{fm}^3$), L_0 is a (technical) length scale (taken to be 1 fm), E the energy of the segment in the Bjorken frame moving with a rapidity y equal to the space-time rapidity η_s, dL is a length element, and k_{Eloss} and E_0 are parameters. We introduce an energy cutoff E_0 to have sufficient energy loss for slowly moving segments.

A string segment will contribute to the bulk (type A segment), when its energy loss is bigger than its energy, i.e.,

$$\Delta E \geqslant E. \quad (2)$$

All the other segments are allowed to leave the bulk (type B or C segments). Only the bulk segments are used to determine the initial conditions for hydrodynamics, following the same procedure as explained in Ref. [8] (with some new elements, as discussed in the next chapter). Starting from this initial condition, the bulk matter will evolve according to the equations of ideal hydrodynamics until hadronization, which occurs at some hadronization temperature T_H [8]. Hadronization means that we change from matter description to particle description, but hadrons still interact among each other, realized via a hadronic cascade procedure [21], already discussed in Ref. [8].

After having performed the hydrodynamic expansion, we have to come back to the string segments that escape the bulk because their energy is bigger than the energy loss. We employ a formation time: the string segments are formed at times t distributed as $\exp(-t/\gamma\tau_{\text{form}})$, with some parameter τ_{form}, which is taken to be 1 fm/c. If the formation time is such that the segment is produced outside the hadronization surface defined by T_H, the segment will escape as it is (type B segment).

Most interesting are the segments that are formed inside but still escape, because they have $E > \Delta E$. These are type C segments. They escape, but their properties change. Actually such a segment leaves matter at the hadronization surface at a particular space-time point x, which is characterized by some collective flow velocity $\vec{v}(x)$. We assume that the string breaking in this case is modified such that the quark and antiquark (or diquark) necessary for the string breaking are taken from the flowing fluid rather than being produced via the Schwinger mechanism. So the new string segment is composed of a quark and antiquark (diquark) carrying the flow velocity, and the string piece in between, which has not been changed. This string piece may or may not carry large momentum, depending on whether it is close to a kink or not, the former possibility shown in Fig. 7.

In any case, due to the fluid-jet interaction, the properties of this segment change drastically compared to the normal fragmentation:

(i) The quark and antiquark (or diquark) from the fluid provide a push in the direction of the moving fluid.
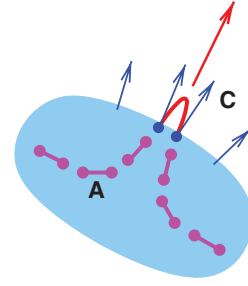

FIG. 7. (Color online) A type C segment picks up quark and antiquark from the fluid, carrying momenta and flavor according to the fluid properties (fluid-jet interaction).

(ii) The quark (antiquark) flavors are determined from Bose-Einstein statistics, with more strangeness production compared to the Schwinger mechanism.

(iii) The probability p_{diq} to have a diquark rather than an antiquark will be bigger compared to a highly suppressed diquark-antidiquark breakup in the Schwinger picture (p_{diq} is a parameter).

Our procedure has four parameters: k_{Eloss} (=0.042), E_0 (=6 GeV), τ_{form}(=1 fm/c), p_{diq}(=0.22). It allows to cover in a single scheme the production of jets, of bulk, and the interaction between the two.

IV. FORMATION TIMES

A crucial ingredient to the mechanism of fluid-jet interaction is the formation time of jet hadrons (the hadrons which leave the fluid). The probability distribution of the formation times t of jet hadrons with gamma factors γ is given as

$$\text{prob} \sim \exp\left(-\frac{t}{\gamma\tau_{\text{form}}}\right), \quad (3)$$

(we use $\tau_{\text{form}} = 1$ fm/c). The probability of having a formation point inside the fluid is obtained as an integral over Eq. (3),

$$1 - \exp\left(-\frac{t_{\text{max}}}{\gamma\tau_{\text{form}}}\right), \quad (4)$$

with t_{max} being the time corresponding to a formation at the fluid surface. Rather than making a simulation, we are going to present a very simple formula providing a rough estimate of the p_t dependence of this probability. For a collision of two Pb nuclei in some centrality interval, characterized by the mean impact parameter b, we use $ct_{\text{max}} = r_{\text{Pb}} - b/2$, where r_{Pb} is the radius parameter used in the Wood-Saxon distribution of nucleons. Considering transversely moving hadrons of mass m, we have $\gamma \approx p_t/mc$. The estimate P_{inside} of the probability to form (pre)hadrons inside the fluid is

$$P_{\text{inside}} = 1 - \exp\left(-\frac{(r_{\text{Pb}} - b/2)\,m}{p_t\,\tau_{\text{form}}}\right). \quad (5)$$

In Fig. 8, we show the result for the 0–5% and the 20–30% most central events in Pb-Pb collisions at 2.76 TeV, using $c\tau_{\text{form}} = 1$ fm, $mc^2 = 1$ GeV, $r_{\text{Pb}} = 6.5$ fm, and for the average impact parameters $b = 1.8$ fm (0–5%) and $b = 7.8$ fm (20–30%).
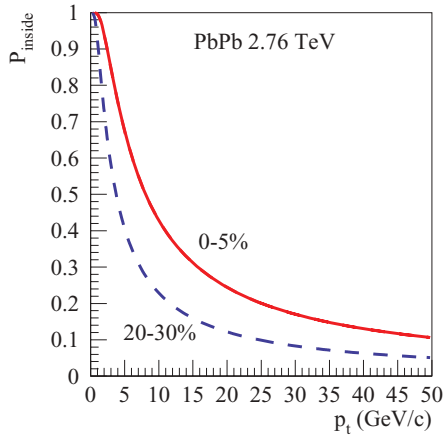
FIG. 8. (Color online) The estimate P_{inside} to form (pre)hadrons inside the fluid, as a function of p_t, for Pb-Pb collisions at 2.76 TeV. We show the curves for the 0–5% and the 20–30% most central events.

By construction, the probability $P_{\text{fluid-jet}}$ of having a fluid-jet interaction is equal to the probability of forming (pre)hadrons inside the fluid, so its estimate is given by P_{inside}. From Fig. 8, we see that the probability is quite large for intermediate values of p_t, but even large values (50 GeV/c) are significantly affected. Whether the effect of the interaction can be seen in some observable is a different question and will be discussed later.

Several authors have already discussed about "in-medium hadronization", see for example Ref. [22], where one also finds an overview about earlier models on this subject.

V. HYDRODYNAMICS

The bulk matter extracted as described above provides the initial condition for a hydrodynamic evolution. As explained in Ref. [8], we compute the energy momentum tensor and the flavor flow vector at some position x (at $\tau = \tau_0$) from the four-momenta of the bulk string segments. The time $\tau = \tau_0$ is as well taken to be the initial time for the hydrodynamic evolution. This seems to be a drastic simplification, the justification being as follows: we imagine to have a purely longitudinal scenario (described by flux tubes) until some proper time $\tau_{\text{flux}} < \tau_0$. During this stage there is practically no transverse expansion, and the energy per unit of space-time rapidity does not change. This property should not change drastically beyond τ_{flux}, so we assume it will continue to hold during thermalization between τ_{flux} and τ_0. So although we cannot say anything about the precise mechanism that leads to thermalization, and therefore we cannot compute the real $T^{\mu\nu}$, we expect at least the elements T^{00} and T^{0i} to stay close to the flux tube values, and we can use the flux tube results to compute the energy density. Only T^{ij} will change considerably, but this does not affect our calculation much.

We employ three-dimensional ideal hydrodynamics as described in Ref. [8], with some modification to be discussed in the following. As in Ref. [8], we construct the equation of state as

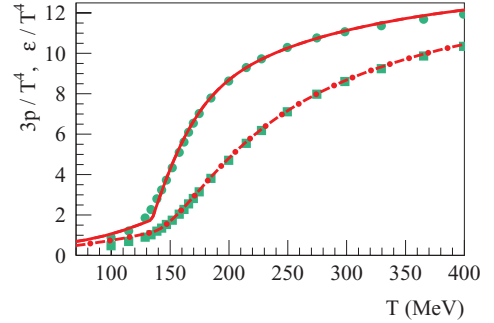$$p = p_Q + \lambda(p_H - p_Q), \qquad (6)$$

FIG. 9. (Color online) Energy density and pressure versus temperature, for our equation of state (lines) compared to lattice data [23] (points).

where p_H is the pressure of a resonance gas, and p_Q the pressure of an ideal quark gluon plasma, including bag pressure. We use an updated λ

$$\lambda = \exp(-z - 3z^2)\Theta(T - T_c) + \Theta(T_c - T), \qquad (7)$$

with

$$z = x/(1 + x/0.77), \quad x = (T - T_c)/\delta, \qquad (8)$$

using $\delta = 0.24 \exp(-\mu_b^2/0.4^2)$. The new λ provides an equation of state in agreement with recent lattice data [23], see Fig. 9.

Apart of the new equation of state, we use the same procedure to obtain energy density and pressure from the string segments, as described in Ref. [8]. However, doing the calculation for Pb-Pb collisions at 2.76 TeV, we get too much elliptical flow (20–30%), a hint that one should include viscosity. Taking the usual small radii of the elementary flux-tubes, we get extremely strongly fluctuating energy densities (in the transverse plane). Viscosity will quickly reduces these strong fluctuations. We try to mimic viscous effects by taking artificially large values of the flux tube radii (we take 1 fm), in
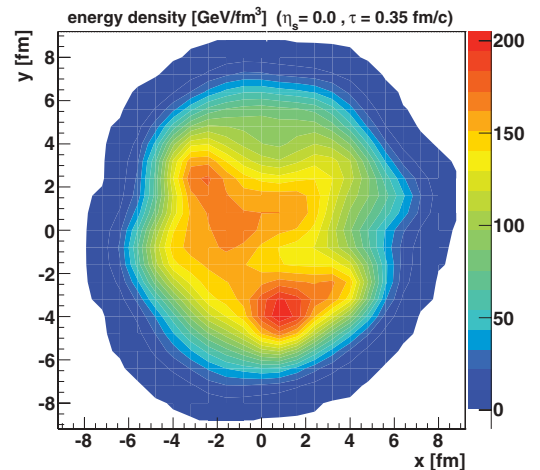

FIG. 10. (Color online) Initial energy density in a central Pb-Pb collision at 2.76 TeV, at a space-time rapidity $\eta_s = 0$, as a function of the transverse coordinates x and y. We take artificially large values of the flux tube radii—which provides relatively smooth initial conditions—to mimic viscous effects.

order to get smoother initial conditions. This has the effect of reducing the elliptical flow by 20–30%, as needed. In Fig. 10, we show an example of such an initial energy density.

VI. CENTRALITY DEPENDENCE OF THE MULTIPLICITY AND FAKE SCALING LAWS

As a very first check of the approach, we consider the centrality dependence of the charged particle yield. Although very basic, there is quite some confusion about this quantity. Whereas hard processes scale roughly with the number of binary nucleon-nucleon collisions (in a simple geometrical picture), the centrality dependence of the charged particle yield (dominated by low p_t) is very different: it looks more like a scaling with the number of participating nucleons. This reminds us of the well-known wounded nucleon model, which has a physical meaning—at low energies the projectile and target nucleons are excited (wounded), and this is the main source of particle production.

Amazingly, this approximate participant scaling holds also at higher energies, the centrality dependence at the LHC is almost identical to the one at the RHIC [24]. This is quite strange, since one might believe that at higher energies hard processes dominate, so one could expect more binary scaling. But this is not the case.

What do we get in the multiple scattering approach? In Fig. 11, we plot the yield per participant ($dn/d\eta(0)/\mathrm{Npart}$) as a function of the centrality. Npart is the number of participating nucleons. As in the data [25], we obtain a moderately increasing yield per participant. How can this happen? How can one get something like a wounded nucleon result at the LHC? In the model we can of course easily check the relative contribution of particle production from remnant decays.

In Fig. 12, we plot the relative fraction of particle production from remnants as a function of the rapidity. As expected, remnant particle production is important at large rapidities, but the contribution at midrapidity is close to zero. So the physical mechanism of soft particle production is not a wounded nucleon picture.

In our approach, the source of particle production is the flux tubes, originating from elementary scatterings, which are in principle proportional to the number of binary nucleon-
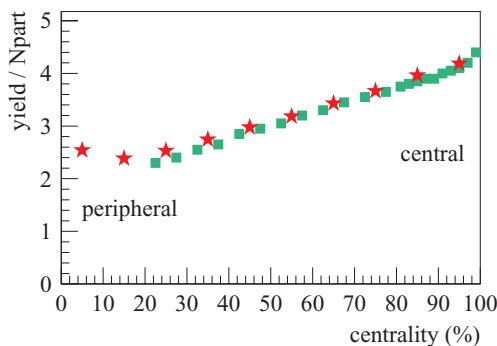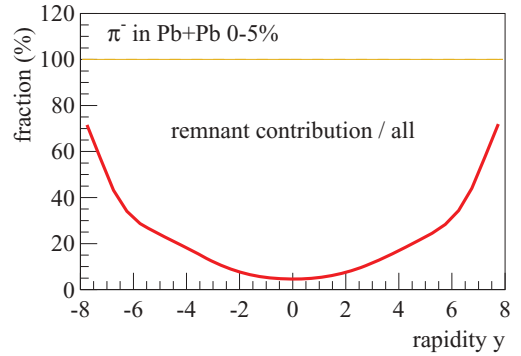

FIG. 12. (Color online) Relative fraction of particle production from remnants versus rapidity. The contribution from remnants at midrapidity is very small.

nucleon collisions. But there are important effects due to energy conservation and shadowing, discussed in detail in [8,9]. In our multiple scattering approach (which determines the initial conditions), the complete AA scattering amplitude is expressed in terms of elementary contributions, which are parton ladders, later showing up as strings. Each parton ladder is characterized by the light cone momentum fractions x_k^+ and x_k^- of the ladder ends, which are the outer partons of the ladder, see Fig. 13 (also transverse momenta are considered, but not discussed here).

It is a unique feature of our approach that we do a precise bookkeeping of energy and momentum: For each nucleon (projectile or target) the initial energy-momentum has to be shared by all the ladders connected to this nucleon and the nucleon remnants, i.e., for all nucleons i we have

$$\sum_{\substack{\text{all ladders } k \\ \text{connected to nucleon } i}} x_k^\pm + x_{\mathrm{remn}\,i}^\pm = 1, \qquad (9)$$

where $x_{\mathrm{remn}\,i}^\pm$ is the momentum fraction of the nucleon remnant i. These are very strong conditions, which affect the results substantially (see Ref. [9]).

The most important consequence relevant for our discussion here is the fact that parton ladders leading to low p_t particles are

FIG. 11. (Color online) Centrality dependence of the charged particle yield. Calculations (stars) are compared to ATLAS data [25] (circles).
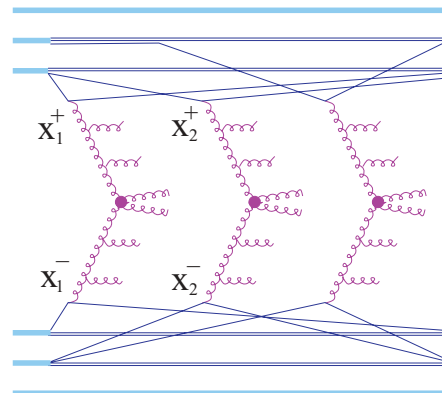

FIG. 13. (Color online) Energy sharing in AA scatterings. The sum of all ladder end light cone momentum fractions $x_k^\pm$ linked to a given remnant and the remnant fraction $x_{\mathrm{remn}\,i}^\pm$ have to add up to unity.
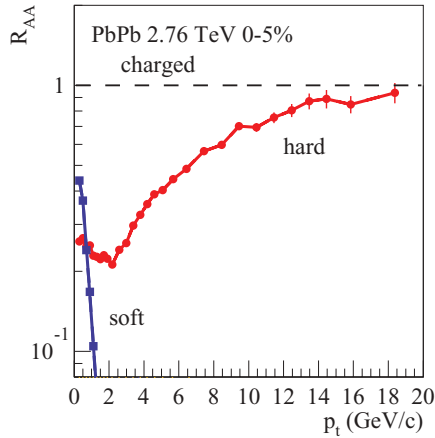
FIG. 14. (Color online) Nuclear modification factor $R_{AA} = N_{\text{coll}}^{-1} (dn_{AA}/dp_t) / (dn_{pp}/dp_t)$ vs transverse momentum p_t, showing the breaking of binary scaling at low p_t (due to energy conservation). The resulting approximate participant scaling at low p_t is a pure coincidence.

suppressed compared to what is expected from binary scaling. We will get a nuclear modification factor, which is less than one at low p_t, as shown in Fig. 14 for central Pb-Pb collisions at 2.76 TeV. So although particle production at central rapidities in very high energy collisions is dominated by binary scattering (providing the initial energy density), particle production does not increase proportional to the number of binary scatterings, due to energy conservation.

It is absolutely necessary that binary scaling is broken at low p_t, because it is simply an experimental fact. The usual explanation is a two component picture: hard scattering at high p_t, which shows binary scaling and a soft component that scales as the number of participants. In our picture, binary collisions determine everything. But certain binary collisions are suppressed due to energy conservation, leading to a deviation from $R_{AA} = 1$.
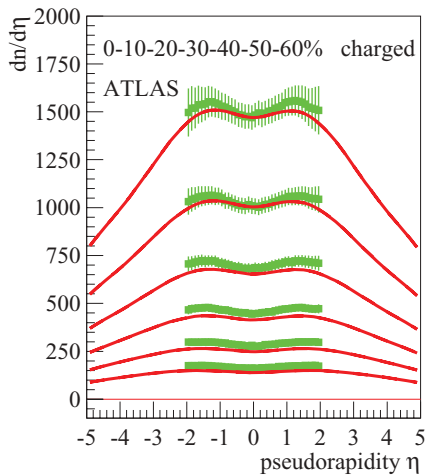

FIG. 15. (Color online) Pseudorapidity distributions of charged particles for different centralities. The lines are calculations, the circles are ATLAS data [25], see text.
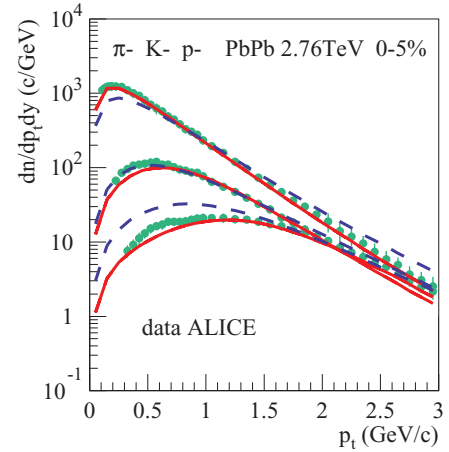

FIG. 16. (Color online) Transverse momentum distributions of (from top to bottom) negative pion, kaons, and protons, in the 0–5% most central Pb-Pb collisions at 2.76 TeV. We show the full calculation (solid lines) and the ones without hadronic cascade (dashed lines), compared to ALICE data (circles) [26].

We will discuss the p_t dependence of R_{AA} in the next section. Here we present for completeness the pseudorapidity distributions of charged particles for different centralities (see Fig. 15) where we compare our calculation with data from ATLAS [25].

VII. TRANSVERSE MOMENTUM DEPENDENCE OF PARTICLE YIELDS: IMPORTANCE OF HADRONIC RESCATTERING OF SOFT AND JET HADRONS

We first investigate particle production at low transverse momenta. In Figs. 16–18, we show transverse momentum distributions of pions, kaons, and protons, for central and semiperipheral Pb-Pb collisions at 2.76 TeV. We compare the full calculation including hydrodynamic evolution and hadronic final state cascade (solid lines) with the calculation without cascade (dashed lines) and with data from ALICE [26].

In order to understand the results, one has to recall that not only the soft particles produced from the fluid may interact, but
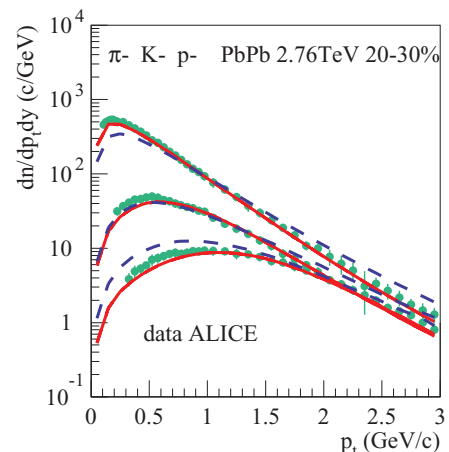

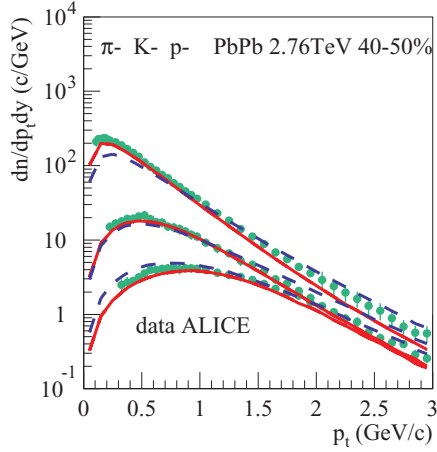FIG. 17. (Color online) Same as Fig. 16, but 20–30% most central.

FIG. 18. (Color online) Same as Fig. 16, but 40–50% most central.

also the jet particles having enough energy to escape the fluid may interact with these soft particles. In particular intermediate p_t jet particles are candidates, because their formation time will produce them just in the high density hadronic region. Let us discuss the consequences of these interactions, by comparing the solid and dashed curves in the figures. We see in particular in Fig. 16 a strong reduction of protons at low p_t due to hadronic rescattering, which can be attributed to proton-antiproton annihilation among the soft hadrons. We see also a sizable increase of pion production at low p_t, which is due to inelastic rescatterings of jet hadrons with soft ones.

In Figs. 16–18, we only show results up to 3 GeV/c, because this is the range where data on protons, pions, and kaons are available. It is nevertheless interesting to know the effect of jet-soft scattering beyond 3 GeV/c. We therefore plot in Fig. 19 the ratio of the full calculation to the one without hadronic cascade, for the p_t spectra of charged particles (dominated by pions) in central Pb-Pb collisions at 2.76 TeV, up to 20 GeV/c. There is a big effect at intermediate values of p_t—up to 20 GeV/c. In other words, jet-soft rescattering is very

FIG. 20. (Color online) Transverse momentum dependence of $1 - R$ (red dots), with R being the ratio plotted in Fig. 19. The dashed line is the estimate P_{inside} of the probability to produce a jet hadron inside the fluid.

important in this range. Similar observation have already been made in Ref. [27] for Au-Au collisions at the RHIC.

The big effect of the jet-soft interaction can be understood by plotting $1 - R$, with R being the ratio (with/without cascade) plotted in Fig. 19, together with the probability estimate P_{inside} to produce a jet (pre)hadron inside the fluid, see Fig. 20. These early produced hadrons go through the dense hadronic phase (of soft hadrons), and P_{inside} is therefore also a measure of the probability of having a jet-soft interaction. We see indeed

$$1 - R = P_{inside}, \qquad (10)$$

at large p_t (in absolute terms, without adding factors). Even though we are running out of statistics, it is clear from the above discussion that the effect goes well beyond 20 GeV/c.

To compare the p_t spectra with experimental data, one uses often the so-called nuclear modification factor R_{AA},
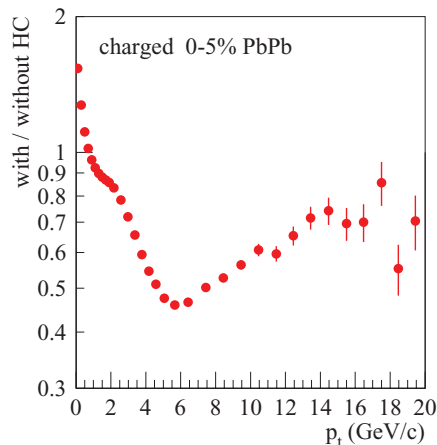

FIG. 19. (Color online) Transverse momentum dependence of the ratio of the full calculation to the one without hadronic cascade, for charged particle production in the 0–5% most central Pb-Pb collisions at 2.76 TeV.
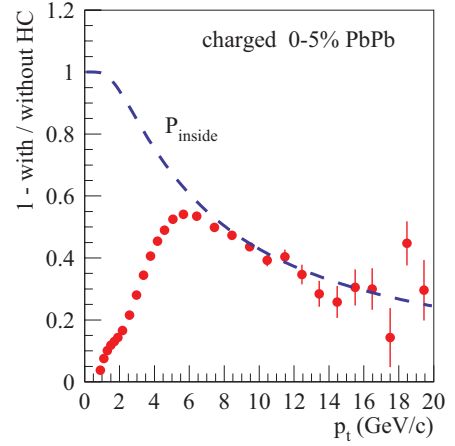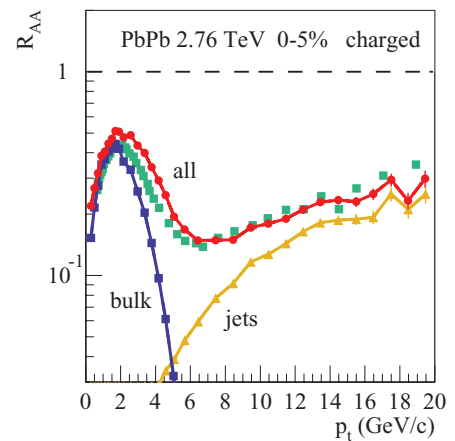

FIG. 21. (Color online) The nuclear modification factor in Pb-Pb at 2.76 TeV vs p_t: We compare data [28] (squares) with the full calculation (red line + circles) and its jet contribution (yellow line + triangles), as well as the bulk (hydro) contribution of a calculation without hadronic cascade (blue line + squares).
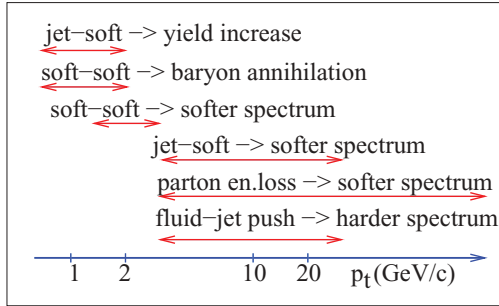
FIG. 22. (Color online) Secondary interactions. The red arrows indicate the p_t ranges that are affected.

which is the ratio of the inclusive transverse momentum spectrum of particles in nucleus-nucleus scatterings over the proton-proton ones, normalized by the number N_{coll} of binary collisions. Doing this procedure, we obtain the curves shown in Fig. 21, where we plot our simulation results for charged particle production together with the data from ALICE [28]. We show the full model, including hydrodynamic evolution and final state hadronic cascade [21] and its jet contribution from the string segments that escaped from the bulk and did not rescatter. We also show the bulk contribution (originating from the hadronized fluid) from the calculation without final state hadronic cascade. The two latter curves do not add up to give the full result; the difference is due to the secondary interactions discussed earlier:

    (i) Fluid-jet interaction, pushing the jet hadrons at intermediate p_t to higher transverse momenta.

   (ii) Jet-soft interactions between jet hadrons and soft ones from fluid freeze-out.

There are also soft-soft interactions (among soft hadrons from fluid freeze-out), which are important for baryon yields, but not so much for the charged particle results.

From the above discussion it is clear that even considering elementary quantities as charged particle yields, it is difficult to make any quantitative analysis without considering these secondary interactions. We sketch the different interactions in Fig. 22.

VIII. DIHADRON CORRELATIONS IN PB-PB AT 2.76 TEV

Our prescription for bulk-jet separation and interaction should also strongly affect dihadron correlations, which provide much more information than simple spectra. With all parameters (k_{Eloss}, E_0, τ_{seg}, p_{diq}) being fixed from the considerations in the last section, we now compute dihadron correlation functions defined as

$$R(\Delta\eta, \Delta\phi) = \frac{M}{S} \times \frac{S(\Delta\eta, \Delta\phi)}{M(\Delta\eta, \Delta\phi)}, \qquad (11)$$

where S is the number of pairs in real events, and M the number of pairs for mixed events.

As an example, we show in Fig. 23 the correlation function for the p_t of the trigger particle (p_t^{trigg}) in the interval 4.5–5.5 GeV/c and the p_t of the associated particle (p_t^{assoc}) in the range
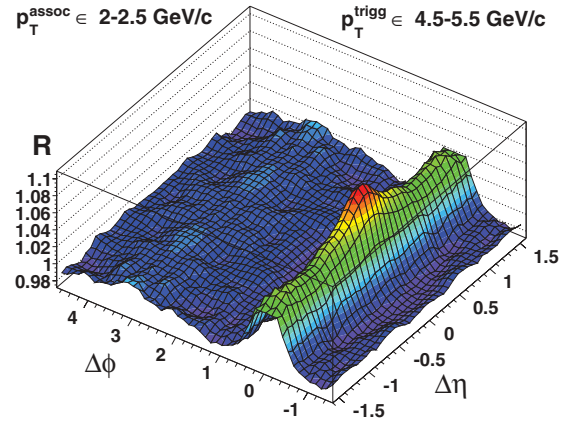

FIG. 23. (Color online) Calculated dihadron correlation function for p_t^{trigg} in the interval 4.5–5.5 GeV/c and p_t^{assoc} in the range 2–2.5 GeV/c in the 0–10% most central Pb-Pb collisions at 2.76 TeV.

2–2.5 GeV/c, in the 0–10% most central Pb-Pb collisions at 2.76 TeV. Besides the jet peak at $\Delta\phi = 0$ and $\Delta\eta = 0$, we clearly identify a completely flat ridge over the full range in $\Delta\eta$ at $\Delta\phi = 0$.

The reason for the ridge structure is the fact that there is an azimuthal asymmetry of the initial energy density (see Fig. 10). Although the energy density is biggest around space-time rapidity $\eta_s = 0$ and drops fast toward forward and backward η_s, the shape of the asymmetry is preserved. This leads finally to an asymmetric flow, again very similar at different values of η_s, and this makes the long-range correlation at $\Delta\phi = 0$.

The smooth η_s dependence of the energy density in our approach (see Fig. 24) is due to the fact the energy density is calculated from flux tubes. And these flux tubes have to be treated correctly as continuous longitudinal objects (as we do). In an earlier version, we treated flux tubes via the randomly (in η_s) distributed flux-tube segments, obtained from a string fragmentation procedures. This gives a bumpy structure in η_s—the ridge is not flat anymore but has a Gaussian shape.
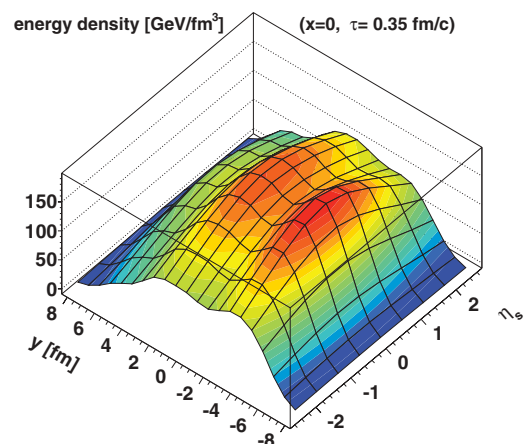

FIG. 24. (Color online) The energy density for a single event in a central Pb-Pb collisions at 2.76 TeV as a function of the longitudinal variable η_s and the transverse one y (and for $x = 0$).
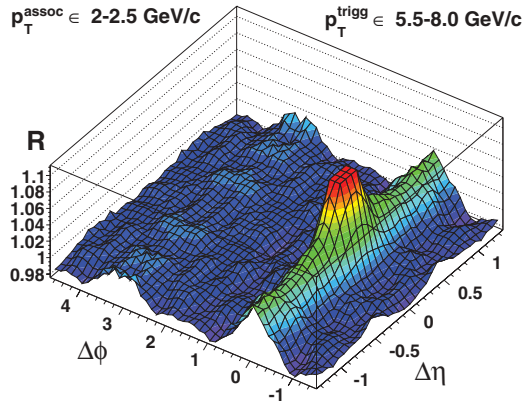
FIG. 25. (Color online) Calculated dihadron correlation function for $p_t^{\rm trigg}$ in the interval 5.5–8.0 GeV/c and $p_t^{\rm assoc}$ in the range 2–2.5 GeV/c in the 0–10% most central Pb-Pb collisions at 2.76 TeV.

So the flux-tube basis is an essential ingredient for obtaining a perfect ridge shape, as observed in the data.

In Fig. 25, we show a correlation function for $p_t^{\rm trigg}$ in the interval 5.5–8.0 GeV/c and $p_t^{\rm assoc}$ in the range 2–2.5 GeV/c, again in the 0–10% most central Pb-Pb collisions at 2.76 TeV. Although the trigger p_t is too large to originate from freeze-out (from the flowing fluid), one still observes a ridge structure, which is due to the fluid-jet interaction. Let us consider again the situation of an initial azimuthal anisotropy in the energy density, which is transported into a corresponding anisotropy in the flow, as discussed earlier. We sketch in Fig. 26 the (somewhat exaggerated) situation of a triangular transverse flow pattern with maximal flow around $\phi = 0°$, 120°, and 240° (with respect to the y axis). The flow maxima are indicated by blue arrows. Again it is very important that this flow pattern is (not necessarily in magnitude, but in shape) very similar at different longitudinal positions, in the figure indicated by the two transverse planes **P** and **P'**, corresponding to two different space-time rapidities η_s and η_s'. A soft hadron (**S**) produced at η_s at the fluid surface close to the position of maximal flow (for example at $\phi = 0°$), will be boosted by the latter one and
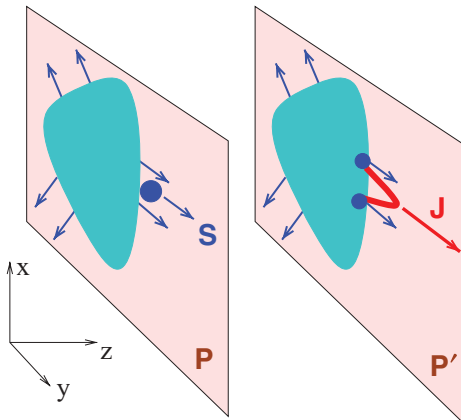

FIG. 26. (Color online) Sketch of two cuts of the fluid volume corresponding to the space-time rapidities η_s and η_s', the two corresponding transverse planes being **P** and **P'**. We show the example of a triangular flow pattern, the same at η_s and η_s'.
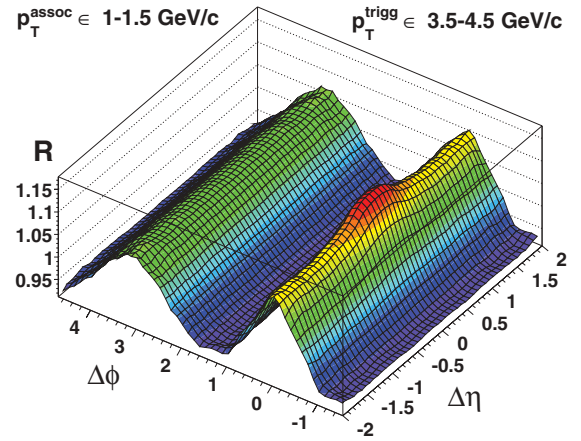

FIG. 27. (Color online) Calculated dihadron correlation function for $p_t^{\rm trigg}$ in the interval 3.5–4.5 GeV/c and $p_t^{\rm assoc}$ in the range 1–1.5 GeV/c in the 40–50% most central Pb-Pb collisions at 2.76 TeV.

therefore carry information about this flow. A jet hadron (**J**) produced at η_s' at the same angle ($\phi = 0°$) close to the surface, will pick up a quark and an antiquark, both carrying flow, which adds the corresponding transverse momentum to the p_t of the string segment (red element in the figure). It is the same flow that affects the jet hadron at η_s' and the soft hadron at η_s, which creates the dihadron correlation at $\Delta\phi = 0$, the ridge. The correlation remains visible, even when the flow contribution to the jet hadron is only 10%, this is why the correlation is still present even for trigger transverse momenta beyond 10 GeV/c.

We will now discuss some examples of semiperipheral Pb-Pb collisions at 2.76 GeV/c. In Fig. 27, we show the correlation function for $p_t^{\rm trigg}$ in the interval 3.5–4.5 GeV/c and $p_t^{\rm assoc}$ in the range 1–1.5 GeV/c, in the 40–50% most central Pb-Pb collisions at 2.76 TeV. It can be clearly seen from the figure that the elliptical flow [$\sim \cos(2\Delta\phi)$] is dominant, besides the jet peak at $\Delta\eta = 0$, $\Delta\phi = 0$. But also here higher order harmonics [$\sim \cos(i\,\Delta\phi)$] contribute, as we will discuss later. In Fig. 28, we show another example of a correlation function for semi-peripheral collisions, with somewhat bigger trigger p_t. We use $p_t^{\rm trigg}$ in the interval 5.5–8.0 GeV/c and $p_t^{\rm assoc}$ in the range 2–2.5 GeV/c. The $\Delta\eta$ range is chosen smaller to avoid to big statistical fluctuations. The jet contribution becomes dominant in this case, but when we cut off the jet peak, we clearly see a very similar elliptical flow structure as in the previous example. The correlation functions are essentially flat as a function of $\Delta\eta$, for large $\Delta\eta$. One therefore gets complete information about the long-range correlations by integrating over $\Delta\eta$,

$$R(\Delta\phi) = \frac{1}{2(B-A)} \int_{A < |\Delta\eta| < B} R(\Delta\eta, \Delta\phi)\, d\Delta\eta, \quad (12)$$

where we use $A = 0.8$ and the maximum $B = 2$. This function agrees perfectly with its Fourier decomposition,

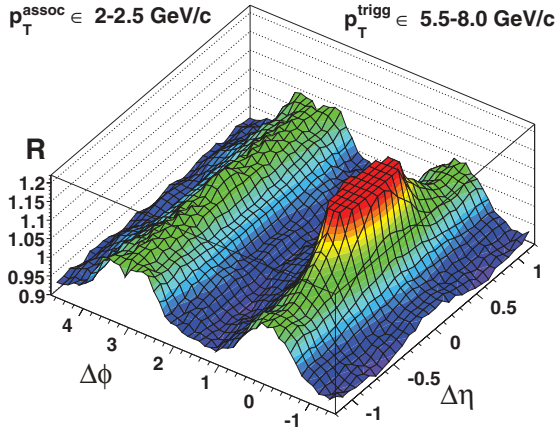$$R(\Delta\phi) = 1 + \sum_{n=1}^{5} 2V_{n\Delta} \cos(n\Delta\phi), \quad (13)$$

FIG. 28. (Color online) Calculated dihadron correlation function for p_t^{trigg} in the interval 5.5–8.0 GeV/c and p_t^{assoc} in the range 2–2.5 GeV/c in the 40–50% most central Pb-Pb collisions at 2.76 TeV. The jet peak has been cut for better visibility.

using the first five terms. This is very convenient, because it allows to discuss the features of the correlation functions for different options for p_t^{trigg} and p_t^{assoc} by simply considering the Fourier coefficients.

In Figs. 29 and 30, we plot some coefficients $V_{n\Delta}$ as a function of p_t^{trigg} for different intervals of p_t^{assoc}. The value of p_t^{trigg} is actually the mean value in a certain interval, the largest interval being 8–15 GeV/c. We compare our simulation (stars) with the results from ALICE [5] (circles).

In the semiperipheral collisions of Fig. 29, we see clearly the dominance of elliptical flow: the $n = 2$ coefficients are by far the largest. Nevertheless, also the higher harmonics contribute. We see in all cases an increase of the coefficients with p_t^{assoc} and with p_t^{trigg} up to values of around 2–3 GeV/c. At the latter values the hydrodynamic flow contributes the most to the correlation between soft hadrons from the fluid.

For higher transverse momenta, the coefficients get smaller, because the correlation between soft particles dies out. But $V_{2\Delta}$ does not at all drop to zero at high p_t because here the correlations between soft and jet particles come into play—the jet particles, which suffered a push by the fluid, as discussed earlier (fluid-jet interaction). The fluid transfers at maximum few GeV/c of transverse momentum to the jet, but this is easily visible in the correlation (even at 20 GeV/c).

The results for semiperipheral collisions are very robust and depend little on model parameters. The most important ingredient is the elliptical initial shape on the energy density, given by the nuclear geometry. The effects depend of course on the flow velocity at freeze-out, but this is not a parameter but itself a robust result (with a maximum around 0.7c). Finally the results depend on the jet formation time, which should be around 1 fm/c (the value we actually took without really attempting a fine tuning).

The $V_{2\Delta}$ coefficients for central Pb-Pb collisions (Fig. 30) are first of all smaller as compared to the semiperipheral ones (note the different scales in Figs. 29 and 30), simply because the dominant effect of large initial ellipticity from the geometry is absent. Here the ellipticity is purely random. Apart from
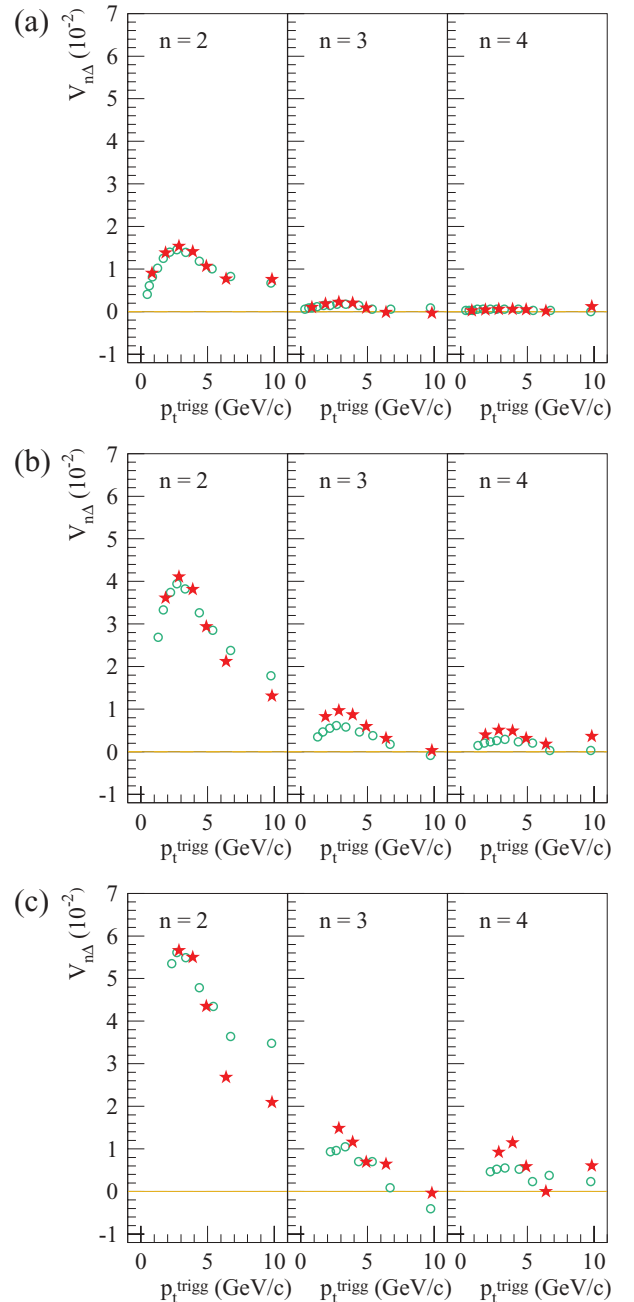

FIG. 29. (Color online) The Fourier coefficients $V_{n\Delta}$ as a function of p_t^{trigg} for p_t^{assoc} within 0.25–0.5 GeV/c (a), 1–1.5 GeV/c (b), 2–2.5 GeV/c (c), in the 40–50% most central Pb-Pb collisions at 2.76 TeV. We compare the ALICE data [5] (circles) with calculations (red stars).

this, we observe the same features as for the semiperipheral collisions: increase with transverse momenta up to 2–3 GeV/c, then decrease. A big difference in central Pb-Pb collisions compared to semiperipheral ones is the fact that the higher harmonics and in particular $V_{3\Delta}$ contribute substantially, because here both elliptical and triangular initial shape are of random origin (and therefore comparable), whereas for more peripheral collisions the geometrical elliptical shape dominates everything else.
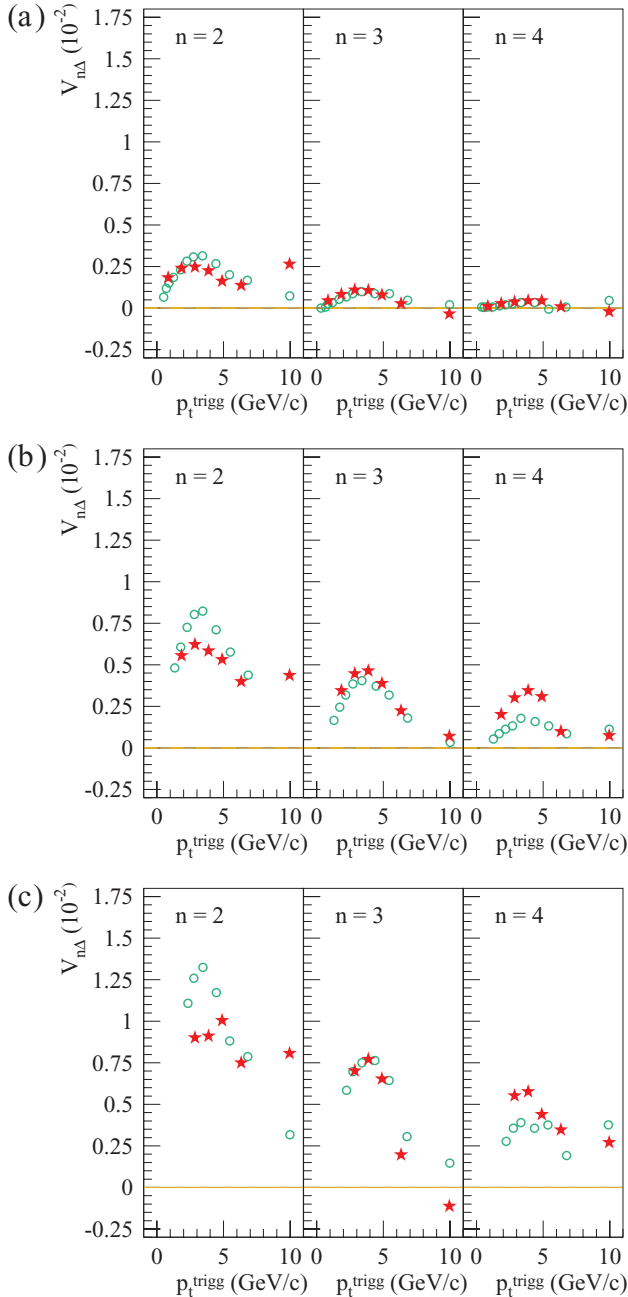
FIG. 31. (Color online) The Fourier coefficients $V_{n\Delta}$ as a function of p_t^{trigg} for p_t^{assoc} within 2–4 GeV/c in the 0–5% most central Pb-Pb collisions at 2.76 TeV. We compare the data [4] (squares) with calculations (red stars).

the role of the flowing fluid, one may get the essential information by considering the elliptical flow coefficient v_2 of single-particle production, which is defined as

$$v_2 = \langle \cos[2(\phi - \phi_{\text{Ref}})]\rangle, \tag{14}$$

where ϕ is the azimuth angle of a particle, and ϕ_{Ref} some reference plane. In Ref. [6], for the particles in the forward (backward) η hemisphere, the reference plane is the event plane angle ϕ^{backward} (ϕ^{forward}), obtained from counting all particles in the opposite hemisphere. The angles are obtained from

$$\phi^{\text{backward/forward}} = \frac{1}{2} \tan^{-1} \frac{\langle \sin 2\phi\rangle}{\langle \cos 2\phi\rangle}, \tag{15}$$

where the average is done in the forward/backward η hemisphere within $3.2 < |\eta| < 4.8$. The v_2 coefficient is then computed as

$$v_2 = \langle \cos[2(\phi - \phi^{\text{forward/backward}})]\rangle. \tag{16}$$

Resolution correction is taken care of by dividing this expression by $R = \sqrt{\langle \cos[2\Delta\phi]\rangle}$, with $\Delta\phi = \phi^{\text{backward}} - \phi^{\text{forward}}$, as in Ref. [6]. Relating particles with the event plane of the opposite hemisphere, we have kind of a long-range correlation, but less clean than using dihadron correlations with a $\Delta\eta > A$ requirement. But as mentioned before, the essential features can be seen as well. In Fig. 32, we plot v_2 as a function of the transverse momentum for different centralities in Pb-Pb collisions at 2.76 TeV. The magnitude of the elliptical flow coefficients increase at low p_t to reach a maximum around 2–3.5 GeV/c and then drop slowly at large p_t.

The behavior at high p_t is the most interesting aspect: even at 10 GeV/c, there is a significant amount of elliptical flow, due to the fluid-jet interaction, which pushes jet particles in the direction of the collective flow at the freeze-out surface (and this effect will continue up to even higher p_t, but we are simply running out of statistics). The high p_t behavior is closely related to the formation time discussion we had earlier. The nonvanishing v_2 at high p_t is mainly due to fluid-jet interactions, so the values should be related to the estimated probability P_{inside} to form the jet hadron inside the fluid, which is equivalent to the fluid-jet interaction probability.

FIG. 30. (Color online) Same as Fig. 29, but for the 0–10% most central Pb-Pb collisions at 2.76 TeV. We compare the ALICE data [5] (circles) with calculations (red stars).

In Fig. 30 it seems that our calculation underestimates $V_{2\Delta}$, in particular for the largest p_t^{assoc} range (2–2.5. GeV). Fortunately, similar data exist from CMS [4], for p_t^{assoc} in the range 2–4 GeV/c in the 0–5% most central Pb-Pb collisions. In Fig. 31, we plot the corresponding coefficients $V_{2\Delta}$ and $V_{3\Delta}$. Here we slightly overpredict the data.

IX. V2 AND FORMATION TIMES

Whereas dihadron correlations provide the most complete information about particle production, in particular concerning
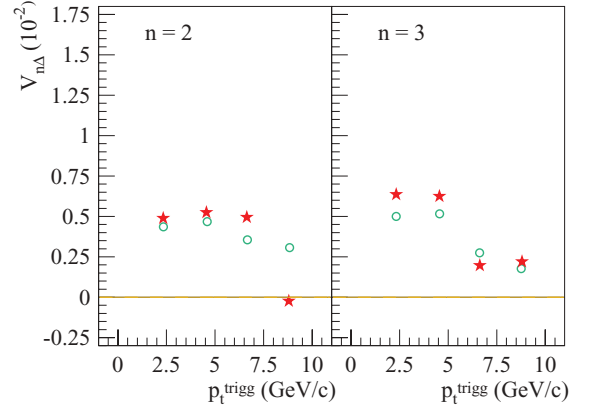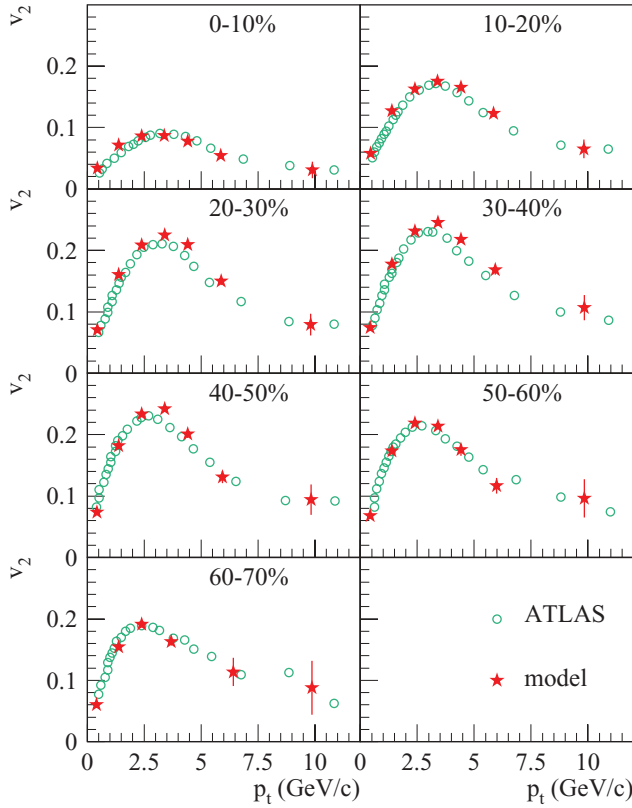
FIG. 32. (Color online) p_t dependence of elliptical flow (defined with respect to the opposite hemisphere subevent plane) for different centralities in Pb-Pb collisions at 2.76 TeV. We compare the ATLAS data [6] (circles) with calculations (red lines).

In Fig. 33, we show P_{inside} (multiplied by an arbitrary factor), together with the calculated and experimental v_2 already show in Fig. 32, which shows that v_2 is indeed proportional to the fluid-jet interaction probability. To compute P_{inside} according to Eq. (5), we use $c\tau_{\mathrm{form}} = 1$ fm, $mc^2 = 1$ GeV, $r_{\mathrm{Pb}} = 6.5$ fm, and $b = 11.5$ fm (50–60%).
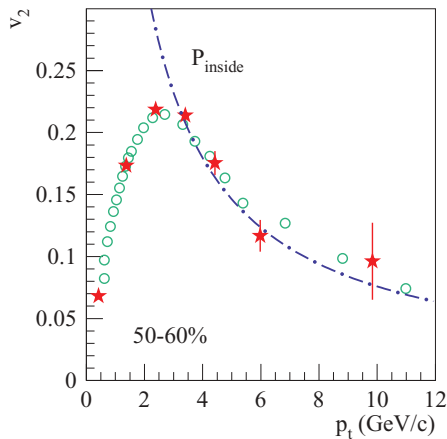

FIG. 33. (Color online) Same data and model calculation as shown in Fig. 32 for the case of 50–60% most central collisions, together with P_{inside}.

Having a finite P_{inside} is a necessary condition to get a substantial v_2 at some large value of p_t, but not a sufficient one. Let us therefore estimate the effect of the fluid-jet interaction on v_2. One may consider a toy model, with soft particle emission due to flow into some preferred azimuthal direction, say ϕ_{flow}. Let us assume a jet hadron getting pushed by the fluid in the direction of ϕ_{flow}, which corresponds to adding some $\vec{p}_t^{\mathrm{soft}}$ to the hard transverse momentum $\vec{p}_t^{\mathrm{hard}}$ of the flux-tube segment. Without loss of generality, we may set $\phi_{\mathrm{flow}} = 0$. The total transverse momentum of the jet hadron is

$$\vec{p}_t^{\mathrm{soft}} + \vec{p}_t^{\mathrm{hard}} = \begin{pmatrix} p_t^{\mathrm{soft}} + p_t^{\mathrm{hard}} \cos(\phi) \\ p_t^{\mathrm{hard}} \sin(\phi) \end{pmatrix} = p_t^{\mathrm{jet}} \begin{pmatrix} \cos\psi \\ \sin\psi \end{pmatrix}, \tag{17}$$

where ψ is the jet hadron direction with respect to the flow direction $\phi_{\mathrm{flow}} = 0$. We have

$$\tan\psi = \frac{p_t^{\mathrm{hard}} \sin(\phi)}{p_t^{\mathrm{soft}} + p_t^{\mathrm{hard}} \cos(\phi)}. \tag{18}$$

Assuming a flat ϕ distribution, the probability distribution for ψ is $(2\pi)^{-1} d\phi/d\psi$, which is in the case of $p_t^{\mathrm{soft}} \ll p_t^{\mathrm{hard}}$ given as

$$1 + \frac{p_t^{\mathrm{soft}}}{p_t^{\mathrm{hard}}} \cos(\psi), \tag{19}$$

which should only be considered for $-\pi/2 < \psi < \pi/2$, since ψ and ϕ_{flow} have to correspond to the same hemisphere. We get anisotropies of the order of $p_t^{\mathrm{soft}}/p_t^{\mathrm{hard}}$, which means at transverse momenta around 10 GeV/c, a soft push as little as 1 GeV/c can produce anisotropies of the order of 10%.

X. COALESCENCE

For many years, different models have been employed to treat particle production at different transverse momentum scales. The so-called intermediate range from 2 to 6 GeV/c has been the domain of coalescence models [29–33], where hadrons are produced by recombining quarks from the plasma, to be distinguished from fragmentation of partons.

In our picture, there are certain aspects which give similar results as coalescence, but it is not a coalescence approach. Already the notion intermediate p_t extends to say 20 GeV/c and not 6. The corresponding transverse momentum of hadrons does not originate from plasma quarks and antiquarks—the main part is coming from the original flux tube. Whereas usual flux tube breaking in vacuum creates quark-antiquark pairs via a tunneling process, the fluid-jet interaction amounts to replacing these quark-antiquark pairs by partons from the plasma. So our jet hadrons finally carry some transverse momentum from fluid partons, but only a small fraction. But this is enough to create for example anisotropies in dihadron correlations. It will also affect strongly baryon to meson rations, as we are going to discuss in a separate publication.

XI. SUMMARY

We presented a theoretical scheme, which accounts for bulk matter, jets, and the interaction between the two. The criterion for bulk-jet separation is based on parton energy loss. But in addition to the latter mechanism, there are very important phenomena that have not been discussed so far: The interaction between jet hadrons and soft ones (from fluid freeze-out), and the interaction between the fluid and jet hadrons at the moment of the creation of the latter ones. Particle production between zero and (at least) 20 GeV/c is affected. We understand quantitatively azimuthal anisotropies in single particle production and dihadron (long-range) correlations at large values of p_t.

ACKNOWLEDGMENTS

[1] B. Abelev *et al.* (STAR Collaboration), Phys. Rev. C **80**, 064912 (2009).

[2] A. Adare *et al.* (PHENIX Collaboration), Phys. Rev. C **78**, 014901 (2008).

[3] B. Alver *et al.* (PHOBOS Collaboration), Phys. Rev. Lett. **104**, 062301 (2010).

[4] CMS Collaboration, S. Chatrchyan *et al.*, J. High Energy Phys. 07 (2011) 076; arXiv:1201.3158.

[5] K. Aamod *et al.* (ALICE Collaboration), Phys. Lett. B **708**, 249 (2012).

[6] G. Aad *et al.* (ATLAS Collaboration), Phys. Lett. B **707**, 330 (2012).

[7] HS06 is the abbreviation for HEP-SPEC-2006, which is a benchmark for measuring CPU performances. The machines we use have an average power of 8.7 HS06 units, this number being referred to as scaling factor.

[8] K. Werner, Iu. Karpenko, T. Pierog, M. Bleicher, and K. Mikhailov, Phys. Rev. C **82**, 044904 (2010).

[9] H. J. Drescher, M. Hladik, S. Ostapchenko, T. Pierog, and K. Werner, Phys. Rep. **350**, 93 (2001).

[10] Y. Nambu, Proc. Intl. Conf. on Symmetries and Quark Models, Wayne State University, 1969 (unpublished).

[11] J. Scherk, Rev. Mod. Phys. **47**, 123 (1975).

[12] C. Rebbi, Phys. Rep. **12**, 1 (1974).

[13] X. Artru, Phys. Rep. **97**, 147 (1983).

[14] D. A. Morris, Nucl. Phys. B **288**, 717, (1987).

[15] K. Werner, Iu. Karpenko, T. Pierog, M. Bleicher, and K. Mikhailov, Phys. Rev. C **83**, 044915 (2011).

[16] K. Werner, Iu. Karpenko, T. Pierog, Phys. Rev. Lett. **106**, 122004, (2011).

[17] M. Cacciari, G. Salam, and G. Soyez, J. High Energy Phys. 04 (2008) 063.

[18] Aad *et al.* (ATLAS collaboration), Eur. Phys. J. C **71**, 1512 (2011).

[19] S. Kretzer, H. L. Lai, F. I. Olness, and W. K. Tung, Phys. Rev. D **69**, 114005 (2004).

[20] R. Baier *et al.*, Nucl. Phys. B **483**, 291 (1997); S. Peigné, AIP Conf. Proc. **1038**, 139, (2008).

[21] M. Bleicher *et al.*, J. Phys. G **25**, 1859 (1999); H. Petersen, J. Steinheimer, G. Burau, M. Bleicher, and H. Stocker, Phys. Rev. C **78**, 044901 (2008).

[22] R. Bellwied and C. Markert, Phys. Lett. B **691**, 208 (2010).

[23] S. Borsanyi *et al.*, J. High Energy Phys. 11 (2010) 77.

[24] CMS Collaboration, S. Chatrchyan *et al.*, J. High Energy Phys. 08 (2011) 141.

[25] G. Aad *et al.* (ATLAS Collaboration), Phys. Lett. B **710**, 363 (2012).

[26] R. Preghenella (ALICE Collaboration), A. Phys. Pol. B **43**, 555 (2012).

[27] K. Gallmeister, C. Greiner, and Z. Xu, Phys. Rev. C **67**, 044905, (2003); W. Cassing, K. Gallmeister, and C. Greiner, Nucl. Phys. A **735**, 277 (2004).

[28] ALICE Collaboration, K. Aamod *et al.*, Phys. Lett. B **696**, 30 (2011).

[29] D. Molnar and S. A. Voloshin, Phys. Rev. Lett. **91**, 092301 (2003).

[30] V. Greco, C. M. Ko, and P. Levai, Phys. Rev. Lett. **90**, 202302 (2003); Phys. Rev. C **68**, 034904 (2003).

[31] R. J. Fries, B. Muller, C. Nonaka, and S. A. Bass, Phys. Rev. Lett. **90**, 202303 (2003); Phys. Rev. C **68**, 044902 (2003).

[32] R. C. Hwa and C. B. Yang, Phys. Rev. C **67**, 034902 (2003); **70**, 024905 (2004).

[33] S. Pratt and S. Pal, Phys. Rev. C **71**, 014905 (2005).